



# Magnetic and microwave studies of high-spin states of single-molecule magnet Ni<sub>4</sub>

Enrique del Barco <sup>a,1</sup>, Andrew D. Kent <sup>a,\*</sup>, En-Che Yang <sup>b</sup>, David N. Hendrickson <sup>b</sup>

<sup>a</sup> Department of Physics, New York University, 4 Washington Place, NY 10003, USA

<sup>b</sup> Department of Chemistry and Biochemistry, University of California San Diego, La Jolla, CA 92093-0358, USA

Received 6 October 2004; accepted 28 December 2004

Available online 21 July 2005

## Abstract

Quantum tunneling of the magnetization in a single-molecule magnet has been studied in experiments that combine microwave spectroscopy (10–50 GHz) with low temperature high sensitivity micro-Hall effect magnetometry ( $T = 0.4$  K). This method enables the monitoring of spin-state populations in the presence of microwave radiation and a direct measure of the energy splitting between low lying high-spin states. We present results that show the level repulsion between such states as a function of magnetic field in the SMM Ni<sub>4</sub> ( $S = 4$ ), which clearly indicates the formation of high-spin superposition states. The absorption linewidths provide a lower bound on the transverse relaxation time ( $\tau_2$ ) or decoherence time of these superposition states of  $\sim 0.5$  ns. Studies as a function of microwave power and magnetic field sweep rate suggest that the energy relaxation rate decreases with increasing longitudinal field and energy splitting between states.

© 2005 Elsevier Ltd. All rights reserved.

**Keywords:** Single-molecule magnet; Quantum tunneling of magnetization; Nanomagnet; Superparamagnet; Quantum computing; Electron paramagnetic resonance; Magnetometry

## 1. Introduction

Single-molecule magnets (SMMs) are very interesting materials for the study of quantum dynamics in nanometer scale magnetic systems. A number of remarkable quantum effects have been observed in SMMs, beginning with the observation of quantum tunneling of the magnetization (QTM) in the SMM Mn<sub>12</sub>-Ac [1–3] and including, among many others, quantum interference in QTM [4] and a crossover between thermally assisted and pure QTM regimes [5]. Recently, a growing focus has been on behavior of the magnetization of SMMs

in presence of microwave radiation [6–10], in part due to recent suggestions that SMMs are potential candidates for quantum information processing [11]. Coherent quantum evolution over a sufficient time is essential for use of SMMs in quantum computers. However, most of the experiments to date have focused on incoherent QTM, where quantum superpositions between high-spin states of the molecules are subject to rapid decay. Decoherence occurs when a quantum system is coupled to an environment with many degrees of freedom, such as lattice vibrations (phonons) or fluctuating magnetic fields (i.e., dipolar or hyperfine fields). This work presents a first step toward the experimental study of coherent QTM in SMMs and the factors that influence the decoherence and energy relaxation times.

We have studied [Ni(hmp)(*t*-BuEtOH)Cl]<sub>4</sub>, henceforth referred to as Ni<sub>4</sub> [12]. The core of each molecule is a distorted cube formed by four Ni<sup>II</sup> magnetic ions

\* Corresponding author. Tel.: +1 212 998 7773; fax: +1 212 995 4016.

E-mail addresses: [delbarco@physics.ucf.edu](mailto:delbarco@physics.ucf.edu) (E. del Barco), [andy.kent@nyu.edu](mailto:andy.kent@nyu.edu) (A.D. Kent).

<sup>1</sup> Present address: Department of Physics, University of Central Florida.

(spin 1), and four alkoxide hmp-oxygen atoms at alternating corners. The molecule has  $S_4$  site symmetry. Ferromagnetic exchange interactions between the four  $\text{Ni}^{\text{II}}$  ions lead to a  $S = 4$  ground state at low temperature, which has been confirmed by high frequency Electron Paramagnetic Resonance (EPR) and magnetic relaxation experiments [12,13]. These molecules have a zero field splitting of the form  $-DS_z^2$ . This uniaxial anisotropy term in the Hamiltonian leads to an energy barrier  $DS^2 \sim 12$  K that separates opposite projections of the spin of the molecule along the easy axis,  $S_z = \pm 4$ .

The spin Hamiltonian of  $\text{Ni}_4$  is to first approximation:

$$H = -DS_z^2 - \mu_B \vec{S} \cdot \hat{g} \cdot \vec{H} + H'. \quad (1)$$

The second term is the Zeeman energy ( $\hat{g} = (g_x, g_y, g_z)$ ,  $\mu_0 = 1$  and  $H$  is in tesla). The last term includes high order transverse anisotropy terms (i.e.,  $C(S_+^4 + S_-^4)$ ). An external magnetic field,  $H_z$ , applied along the easy axis of the molecules tilts the double well potential favoring those spin projections aligned with the field. When the magnitude of the longitudinal field is  $H_z = kD/g\mu_B$  (with  $k$  an integer), spin levels on opposite sides of the barrier have the same energy. These field values are known as *resonant fields*. The inset of Fig. 2 shows the behavior of the lowest states as a function of longitudinal magnetic field in the vicinity of resonance  $k = 0$  ( $H_z = 0$ ). When the system is near this resonance off-diagonal terms in the Hamiltonian, such as a Zeeman term due to an external transverse magnetic field lead to an energy splitting between symmetric,  $|S\rangle$  and anti-symmetric  $|A\rangle$  linear combinations of  $|\text{up}\rangle$  and  $|\text{down}\rangle$  states, known as the tunnel splitting,  $\Delta$ . The frequency of QTM between  $|\text{up}\rangle$  and  $|\text{down}\rangle$  states is proportional to the tunnel splitting ( $f = \Delta/h$ ). It is possible to write the energy eigenstates as:

$$\begin{aligned} |S\rangle &= \frac{1}{2}(|\text{up}\rangle + |\text{down}\rangle), \\ |A\rangle &= \frac{1}{2}(|\text{up}\rangle - |\text{down}\rangle), \end{aligned} \quad (2)$$

where

$$\begin{aligned} |\text{up}\rangle &= \frac{\sqrt{2}}{2} \sum_m (a_m + b_m) |m\rangle, \\ |\text{down}\rangle &= -\frac{\sqrt{2}}{2} \sum_m (a_m - b_m) |m\rangle. \end{aligned} \quad (3)$$

The value of the coefficients,  $a_m$  and  $b_m$ , depend on the external applied field. At zero longitudinal field ( $k = 0$ ) and in the absence of transverse fields, all coefficients are zero except for  $a_{+4}$  and  $b_{-4}$ . In this situation, the two lowest levels are  $|S\rangle = \frac{1}{\sqrt{2}}(|+4\rangle + |-4\rangle)$  and  $|A\rangle = \frac{1}{\sqrt{2}}(|+4\rangle - |-4\rangle)$ , corresponding to superpositions of opposite spin projections along the easy magnetic axis. In the presence of a strong transverse field

this situation changes. Now, the states  $|\text{up}\rangle$  and  $|\text{down}\rangle$  are tilted away from the easy axis but still have well defined and opposite  $z$ -axis magnetizations, provided the transverse field is less than the anisotropy field,  $H_a = 2DS/(g\mu_B) = 4.5$  T.

A transverse field is necessary to increase the tunnel splitting into a range where it is comparable or larger than the thermal energy ( $k_B T$ ). In the experiments described below we use transverse fields from 2.2 to 3.6 T, for which the tunnel splitting ranges from 5 to 30 GHz.

## 2. Experimental

The experiment consists in sweeping an external longitudinal field across resonance  $k = 0$  and measuring the magnetization of the sample in the presence of microwave radiation (see inset of Fig. 2). Photon induced transitions (PIT) between symmetric and anti-symmetric spin-states lead to changes of the average magnetization of the sample when the radiation energy coincides with the energy separation between levels. Note that this is only possible when the longitudinal field is not zero. When  $H_z = 0$ , both symmetric and anti-symmetric superposition states have zero  $z$ -axis projection and therefore transitions between them will not change the magnetization of the sample.

In order to induce transitions between  $|S\rangle$  and  $|A\rangle$  states the magnetic field component of the electromagnetic radiation,  $H_{ac}$ , must be aligned with the easy axis direction,  $\hat{z}$ . In this case, the rate of PITs (at  $T = 0$ ) is given by:

$$\Gamma = \frac{\pi}{2} \left( \frac{g\mu_B}{\hbar} H_{ac} \right)^2 |\langle S|S_z|A\rangle|^2 f(\omega), \quad (4)$$

where  $\langle S|S_z|A\rangle$  is the matrix element coupling the external radiation field and the spin of the molecule. On one hand, this probability depends on the magnitude of the ac field (i.e., the radiation power), which is determined by both the source power and the device that is used to irradiate the sample (i.e., the quality factor of the antenna). On the other hand the PIT probability depends on the magnitude of the external magnetic fields as follows: (1) for a given longitudinal field, the larger the transverse field (i.e., the larger tunnel splitting) the higher the probability, and (2) for a given transverse field, the probability increases as the longitudinal field decreases (see inset of Fig. 3), being maximum for  $H_L = 0$ . However, in this case, as mentioned above, PIT do not induce changes in the magnetization. A picture of the range of longitudinal fields for which PITs are allowed can be seen in the inset of Fig. 2. The departure of the energy splitting from a straight line (i.e., the simple Zeeman splitting), illustrated with the dashed line in this figure is due to the tunnel splitting.

In the experiment we sweep the longitudinal field at a given rate,  $\alpha = dH_L/dt$ , across the resonance, in the

presence of a constant transverse field,  $H_T$ , while we monitor the magnetization. For high transverse fields one finds the equilibrium magnetization,  $M_{\text{eq}}(H_L, H_T, T)$ . However, when the energy difference,  $E$ , between the two states matches the energy of the radiation,  $\hbar\omega$ , PITs change the populations of each state and thus the sample magnetization. This effect is manifested as a dip or peak in the magnetization curve whose shape is determined by  $f(\omega)$ , which is a Lorentzian function:

$$f(\omega) = \frac{1}{\pi} \frac{\tau_2}{1 + (\omega - \omega_0)^2 \tau_2^2}, \quad (5)$$

where  $\omega_0 = E/\hbar$  and  $\tau_2$  is the transverse relaxation time. Therefore, the width of the peak will give us information about the decoherence time.

At a finite temperature,  $T > 0$ , the ratio between equilibrium populations of the two lowest states is  $N_2/N_1 = \exp(-E/k_B T)$ . Any non-equilibrium population will decay exponentially according to  $d(n_2 - n_1)/dt = [(N_2 - N_1) - (n_2 - n_1)]/\tau_1$ , where  $n_1$  and  $n_2$  are the instantaneous level populations and  $\tau_1$  is the energy longitudinal relaxation time. In the presence of radiation the evolution of the populations of these states is determined by the PIT rate,  $\Gamma$ , given in Eq. (4) in the form  $d(n_2 - n_1)/dt = -2\Gamma(n_2 - n_1)$ . Combining these two expressions we find:

$$n_d = n_0 \left( 1 - \frac{1}{1 + 2\tau_1 \Gamma} \right) e^{-(\tau_1 + 2\Gamma)t/\tau_1} + \frac{n_0}{1 + 2\tau_1 \Gamma}, \quad (6)$$

where  $n_d = n_2 - n_1$  and  $n_0 = N_2 - N_1$ . From this is it clear that  $n_0$  must not be zero. In other words, we need to work at a temperature for which the excited state population is small. Taking into account that the lowest temperature we can achieve in our experiment is 0.38 K, we need to work with frequencies of at least  $f = E/\hbar = 10$  GHz, in order to have  $n_0 > 0.7$  (for 20 GHz,  $n_0 = 0.91$ ).

We have used a high sensitivity micro-Hall magnetometer [14] to measure the longitudinal component of the magnetization of a millimeter-sized single crystal of  $\text{Ni}_4$  that is placed over the magnetometer, with one of its faces parallel to the plane of the sensor. A thin superconducting circular loop ( $\phi \sim 2$  mm) is placed perpendicular to the easy anisotropy axis of the crystal (see inset of Fig. 1). This loop shorts the end of a 2.4 mm coaxial line, connecting the inner and outer conductors. The coaxial line is made up of Cu and Stainless Steel sections to minimize power losses ( $\sim 15$  dB) and thermal conduction. The line is about 1.5 m long and connects the loop to an Agilent PNA 50 GHz Vector Network Analyzer. This system allows us to work with frequencies up to 50 GHz and makes possible the characterization of the resonances of the loop. All the measurements were done by using different loop resonances to maximize the power that is converted to ac magnetic field

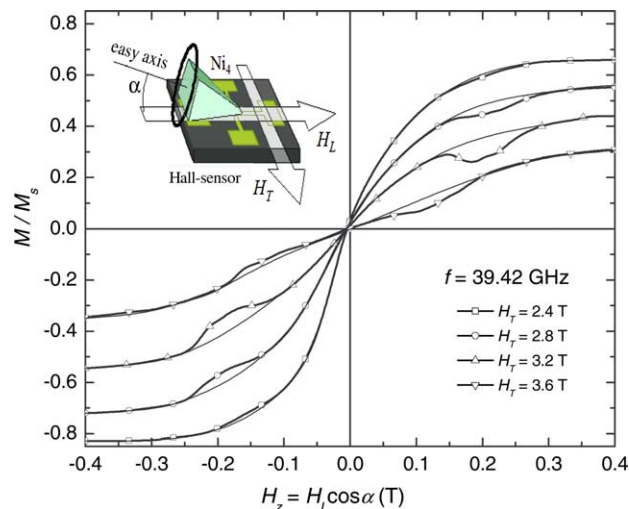


Fig. 1. Several magnetization curves recorded by sweeping the longitudinal field at a constant rate across zero field resonance in the presence of CW microwave radiation of  $f = 39.8$  GHz for transverse fields values from 2.4 to 3.6 T. The thin lines correspond to equilibrium magnetization in the absence of radiation. The inset shows the setup.

at the sample position. A high field superconducting vector magnet was used to apply magnetic fields in arbitrary directions with respect to the axes of the crystal. In this case, both transverse and longitudinal magnetic fields were applied in the plane of the magnetometer. A  $^3\text{He}$  cryostat is used to cool the sample to a temperature of 0.38 K.

### 3. Results and discussion

Fig. 1 shows several magnetization curves measured in presence of continuous wave (CW) microwave radiation of  $f = 39.42$  GHz. The longitudinal magnetic field,  $H_z^2$ , was swept at a constant rate from  $-0.4$  to  $0.4$  T. Different curves correspond to different transverse fields from  $H_T = 2.4$ – $3.6$  T. The thin lines represent the equilibrium magnetizations (or magnetization in the absence of microwave radiation). Deviations of the magnetization from  $M_{\text{eq}}$  are observed (peaks/dips) at opposite polarities of the longitudinal magnetic field<sup>3</sup>, indicating PITs between spin levels with opposite net magnetization. The temperature of the sample was monitored during the whole field sweep and showed variations that

<sup>2</sup> The longitudinal magnetic field,  $H_z$ , represented in Fig. 1 has been calculated taking into account the misalignment,  $\alpha = 20^\circ$ , between the applied field,  $H_L$ , (in the plane of the sensor) and the easy-axis of the single crystal, and is given by the relation  $H_z = H_L \cos \alpha$ .

<sup>3</sup> The small asymmetries observed between the longitudinal field positions and magnitudes of the peak and dip at opposite polarities is due to a second misalignment,  $\theta = 5.3^\circ$ , between  $H_L$  and the projection of the easy axis of the crystal into the plane of the sensor. This misalignment produces variations of the transverse field felt by the molecules when the longitudinal field varies, explaining the asymmetry between PITs at opposite polarities of  $H_z$ .

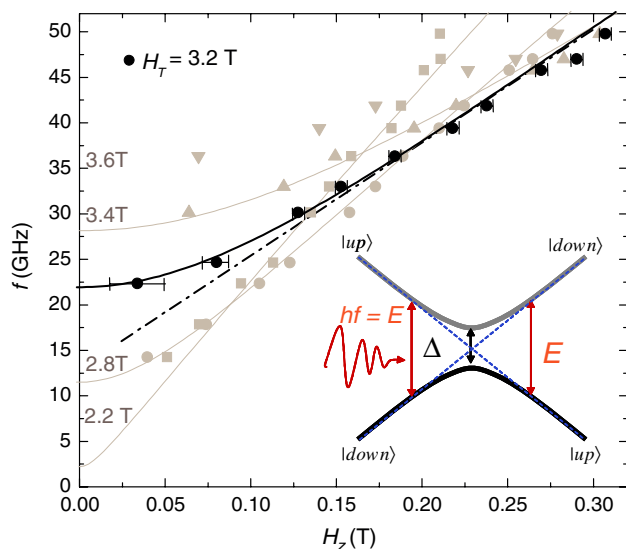


Fig. 2. Frequency-field plot of the positions of the PIT's dips of the sample magnetization. The result corresponding to  $H_T = 3.2$  T has been highlighted (black solid circles) in order to show the curvature of the PIT's frequency-field behavior in the vicinity of zero-field resonance. Grey circles correspond to other transverse field values. The solid lines are fit of the data using Hamiltonian of Eq. (1). The inset shows energies of the lowest lying levels of the  $\text{Ni}_4$  molecule close to zero-field.

were less than 0.01 K at the positions of the peaks and dips. Note that a change of temperature of 1 K would be necessary to explain the magnetization changes observed in the peaks/dips, indicating that these magnetization variations are induced by population changes induced by absorption of microwave radiation and not by heating of the sample. The observed structure of the peaks/dips (each peak/dip is indeed composed by three peaks) is discussed in [10] and has also been observed in high-frequency EPR measurements [13] and ascribed to different  $\text{Ni}_4$  species or microenvironments with slightly different values of the uniaxial anisotropy parameter,  $D$ .

We repeated the same measurements for different microwave frequencies from 14 to 50 GHz for the transverse fields,  $H_T = 2.2$ –3.6 T. For this experiment we chose the microwave powers so that the sample temperature was the same in all the measurements<sup>4</sup>. In Fig. 2 we show the behavior of the PIT dips (positive field polarity) in a frequency-field plot. In this figure results corresponding to  $H_T = 3.2$  T (black solid circles) has been highlighted in order to clearly show the characteristics with microwave frequency and longitudinal field. (Results for negative polarities of  $H_z$  and a more de-

<sup>4</sup> For frequencies over 40 GHz the temperature of the sample was slightly smaller than at lower frequencies due to limitations of the microwave source at high frequencies and higher losses in the coaxial lines. Nevertheless, this temperature difference is not crucial for the analysis of this paper.

tailed discussion can be found in [10].) It is clear that the PIT dip position deviates from the linear behavior (dashed line) on approaching the center of the resonance. This result is a direct measurement of the behavior of the energy difference between the two lowest spin states of the molecule (inset of Fig. 2) and the curvature at the vicinity of the zero-field resonance constitutes an unambiguous signature of quantum superposition states with opposite magnetizations. The solid lines are fits of the data by direct diagonalization of Hamiltonian of Eq. (1) using  $D = 0.765$  K,  $B = 7.9 \times 10^{-3}$  K,  $C = 3.25 \times 10^{-5}$  K,  $g_z = 2.3$ ,  $g_x = g_y = 2.23$ . These values are in excellent agreement with those found from high frequency EPR experiments [13]. This illustrates that the tunnel splitting,  $\Delta$  (at  $H_z = 0$ ), varies from 2 to 35 GHz for transverse fields ranging from 2.2 to 3.6 T [10].

Fig. 3 shows curves corresponding to the difference  $M - M_{\text{eq}}$  for several frequencies from 18 to 47 GHz measured while a transverse field of 3 T was applied. The curves have been normalized by the equilibrium magnetization,  $M_{\text{eq}}(H_z)$ . This normalization allows the behavior of the magnitude of the PIT's dip as a function of the longitudinal field to be seen. The magnitude of the PIT's dip for different field values gives an estimate of the absorption of microwave radiation of a given frequency. The results show that the dip maximum amplitude decreases with field (see dashed line connecting dip's maxima in Fig. 3). From Eq. (4) we know that the maximum amplitude of the PIT's dip, which occurs at  $\omega = \omega_0$ , depends on the magnitude of the microwave field, on the matrix element coupling the external radiation field

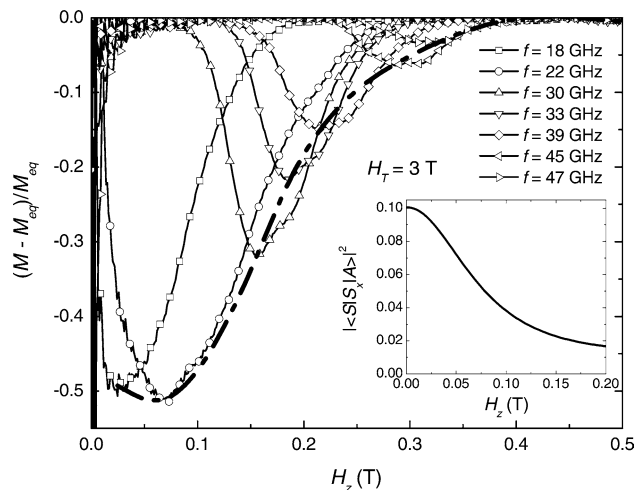


Fig. 3. Normalized change of the magnetization due to PITs at different microwave frequencies in the presence of a 3 T transverse applied field. The dashed-dotted line connecting the dip amplitudes has a minimum at  $\sim 0.06$  T, which is not expected if the amplitude is governed solely by the matrix element in Eq. (4). The inset shows the square of this matrix element as a function of the longitudinal magnetic field for a transverse field of 3 T.

and the spin of the molecule,  $\langle S|S_z|A \rangle$ , and on  $\tau_2$ , through the Lorentzian function of Eq. (5). While  $H_{ac}$  is independent of the longitudinal field and frequency,<sup>4</sup> the matrix element decreases with the longitudinal field as shown in the inset of Fig. 3, having a maximum at zero-field, indicating that the amplitude of the PIT's dip should monotonically decrease with longitudinal field as seen in the experiment. We note that a varying  $\tau_1$  would affect the behavior of the PIT's dips/peaks amplitude since the instantaneous population difference  $n_d = n_1 - n_2$ , and thus the magnetization, are  $\tau_1$ -dependent, as seen in Eq. (6). This could explain the slight decrease of the peak's amplitude observed at  $f = 18$  GHz in Fig. 3, which would be due to an increase in the longitudinal relaxation rate,  $1/\tau_1$ , in the vicinity of the resonance.

A signature of an increase of the longitudinal relaxation time,  $\tau_1$ , with field or frequency is clearly observed in Fig. 4, which shows several  $(M - M_{eq})/M_{eq}$  curves measured at different sweep rates of the longitudinal field and two different sweep directions: from negative to positive (up) and from positive to negative (down). The measurements were done in the presence of microwave radiation of 39.8 GHz and a transverse field of 3.2 T. The curves depend on the field sweep direction. When the field is swept from negative to positive the peak's ( $H_z < 0$ ) amplitude decreases with increasing sweep rate (the peak's width remains almost constant) while the dip's ( $H_z > 0$ ) width increases with increasing sweep rate (the dip's amplitude remains almost constant). The result for the opposite sweep direction is just equivalent but inverted. This broadening of the peaks/

dips with increasing sweep rate is indicative of slow energy relaxation processes of the excited state (antisymmetric state). An estimation of the longitudinal relaxation time, from the width of the peaks shown in Fig. 4, gives  $\tau_1 \sim 13$  s for negative-to-positive sweep direction and  $\tau_1 \sim 19$  s for positive-to-negative sweep direction. The difference in these relaxation times is probably related to the transverse field, which varies slightly with the longitudinal field due to a misalignment of the sample with respect to the applied longitudinal field direction<sup>3</sup>. Moreover, this shows that  $\tau_1$  increases with longitudinal field, and thus with frequency, because the broadening only appears in one side of the peaks/dips (far from the resonance). This trend has also been observed in measurements with pulsed-microwave radiation (see [10] for details).

Relaxation processes must transfer energy to the environment, leading, for example, to generation of phonons or photons. The occurrence of each of these phenomena depends on the energy of the transitions and the temperature of the system (i.e., energy distribution of phonon or photon modes). The extracted relaxation times found here may indicate a very long spin-lattice relaxation time. However, slow relaxation processes could also be associated with poor thermal coupling between the sample and bath. We note that the phase space available for phonon generation increases with frequency. Therefore, since our experiments show that energy relaxation time increases with frequency, this result is not consistent with a spin-phonon bottleneck of the type studied in [15]. These experiments constitute an excellent means for studying the spin-environment coupling that govern quantum dynamics in SMMs.

We also note that the width of the PITs peaks/dips at different microwave powers provide a lower bound on the decoherence time,  $\tau_\phi > 0.5$  ns (see [10]). Interestingly, a very similar decoherence time,  $\tau_\phi = 1$  ns, has been recently reported by Hill et al. [16] through high frequency EPR experiments carried out in a single crystal of  $Mn_4$ -based SMMs ( $S = 9/2$ ), in which exchange interaction between pairs of adjacent molecules (dimers) generate entanglement of the spin states of both molecules.

Improvement of the resonance circuit used to irradiate the sample, higher radiation powers and short pulses of radiation are necessary to carry out spin-echo experiments and to create Rabi oscillations. The Rabi frequency is determined by the magnitude of the ac magnetic field,  $\Gamma_R \approx \frac{g\mu_B}{h} H_{ac} S$ , and in our best case (at present) is of the order of  $\sim 100$  kHz. Antiferromagnetic molecular magnets with an uncompensated electronic or nuclear spin that tracks the Neel vector for readout are also excellent candidates for long coherence times in mesoscopic spin-systems and for use in quantum computation [17,18].

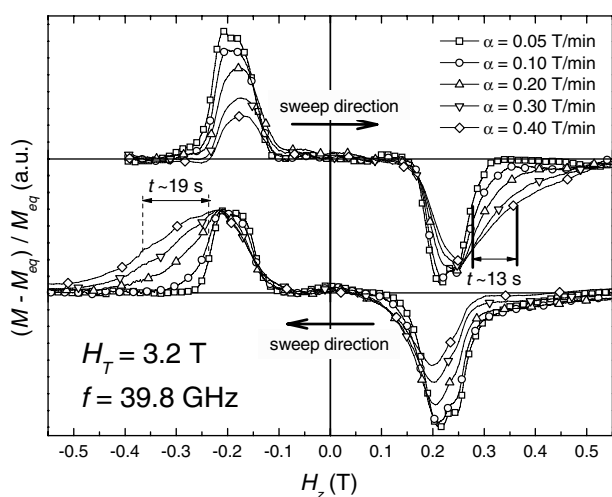


Fig. 4.  $(M - M_{eq})/M_{eq}$  curves for different longitudinal field sweep rates from 0.05 to 0.4 T/min measured in the presence of microwave radiation of 39.8 GHz and a transverse field of 3.2 T. The asymmetric broadening of the peaks/dips for high sweep rates is indicative of a long energy relaxation time which increases with field and thus with frequency.

## Acknowledgements

We acknowledge Eugene Chudnovsky, Dmitry Garanin and Steve Hill for helpful and stimulating discussions of this work. This research was supported by NSF (Grant Nos. DMR-0103290, 0114142, and 0315609).

## References

- [1] J.R. Friedman et al., Phys. Rev. Lett. 76 (1996) 3830.
- [2] J.M. Hernandez et al., Europhys. Lett. 35 (1996) 301.
- [3] L. Thomas et al., Nature (London) 383 (1996) 145.
- [4] W. Wernsdorfer, R. Sessoli, Science 284 (1999) 133.
- [5] L. Bokacheva, A.D. Kent, M.A. Walters, Phys. Rev. Lett. 85 (2000) 4803.
- [6] J. Tejada et al., Appl. Phys. Lett. 84 (2004) 2373.
- [7] L. Sorace et al., Phys. Rev. B 68 (2003) 220407(R).
- [8] W. Wernsdorfer, A. Muller, D. Maily, B. Barbara, Europhys. Lett. 66 (2004) 861.
- [9] M. Bal et al., Phys. Rev. B 70 (2004) 100408.
- [10] E. del Barco, A.D. Kent, E.C. Yang, D.N. Hendrickson, Phys. Rev. Lett. 93 (2004) 157202.
- [11] M. Leuenberger, D. Loss, Nature (London) 410 (2001) 789.
- [12] E.C. Yang et al., Polyhedron 22 (2003) 1727.
- [13] R.S. Edwards et al., J. Appl. Phys. 93 (2003) 7807.
- [14] A.D. Kent, S. von Molnar, S. Gider, D.D. Awschalom, J. Appl. Phys. 76 (1994) 6656.
- [15] I. Chiorescu et al., Phys. Rev. Lett. 84 (2000) 3454.
- [16] S. Hill, R.S. Edwards, N. Aliaga-Alcalde, G. Christou, Science 302 (2003) 1015.
- [17] A. Chiolero, D. Loss, Phys. Rev. Lett. 80 (1998) 169.
- [18] F. Meier, J. Levy, D. Loss, Phys. Rev. Lett. 90 (2003) 047901.